

## Simulations of Galactic Cosmic-Ray transport using data informed 3-dimensional gas reconstructions

---

**Andrés Felipe Ramírez Tapias<sup>a,\*</sup> and Ralf Kissmann<sup>a</sup>**

<sup>a</sup>Universität Innsbruck,

Technikerstraße 25, Innsbruck, Austria

E-mail: [Andres.Ramirez-Tapias@uibk.ac.at](mailto:Andres.Ramirez-Tapias@uibk.ac.at), [ralf.kissmann@uibk.ac.at](mailto:ralf.kissmann@uibk.ac.at)

The interstellar medium of the Milky Way represents a complex coupling of various constituents, where transport and interactions of cosmic rays (CRs) play a major role. They are further influenced by the spatial distribution of CR sources, Galactic gas, starlight, and magnetic fields. As part of a series of Galactic 3D reconstructions, we solve the CR transport problem through the numerical framework PICARD. Here, we introduce 3-dimensional gas distributions for the atomic (HI) and molecular (H<sub>2</sub>) components; reconstructed from direct spectral line measurements for the former, and CO surveys for the latter. These results are studied independently from the standard approach, where the Galactic structures are determined by so called ring models. In this study, CR source distributions are introduced in the simulations as axially symmetric models. As a result, all Galactic structures are defined entirely by the gas reconstructions. Furthermore, the results of CR distributions are used to study gamma-emission, in particular the pion decay and bremsstrahlung components. We compare said components with results obtained by use of the High-Energy Radiative Messengers (HERMES) framework. This shows the difference between the ring and 3-dimensional modeling approaches, where the lack of near-far ambiguity in the latter is of main interest and presents the main advantage of transitioning towards 3-dimensional maps of transport relevant quantities.

38th International Cosmic Ray Conference (ICRC2023)  
26 July - 3 August, 2023  
Nagoya, Japan



---

\*Speaker

## 1. Introduction

Over the last decade new experiments have provided us with new CR data covering energy ranges from the GeV to the TeV scale and beyond. From such data, insights on the nature of CRs and their transport mechanisms can be drawn. In order to understand these observations at the galactic level, the comprehension of the underlying particle acceleration, transport and interactions with the interstellar medium is necessary. This propagation problem is modeled through the CR transport equation and derived by use of numerical simulations. Different frameworks model CR-transport at the galactic scale, such as: GALPROP [10], DRAGON[4] and USINE [7]. These frameworks provide a full numerical solution for transport as a diffusive process. In GALPROP and Dragon, gas distributions are modeled through the introduction of 2D symmetrical ring models, and more recently 3D models [5]. This work will focus on studying the effect of highly resolved 3D gas reconstructions on diffusive transport, by use of the code for diffusive transport PICARD [6].

## 2. Method

In this study, the new gas reconstructions for molecular [9] and atomic [8] hydrogen are introduced into the PICARD framework. Based on different velocity field models (BEG03 and SBM15), two reconstructions for molecular and atomic gas are introduced. For the purpose of adapting the reconstructions for use in our simulations, the gas is interpolated onto the PICARD simulation grid. Figure 1 displays the mean surface mass density of the total ISM gas (HI, H2 and axisymmetric HII) for the two velocity models, as it is loaded into the simulations.

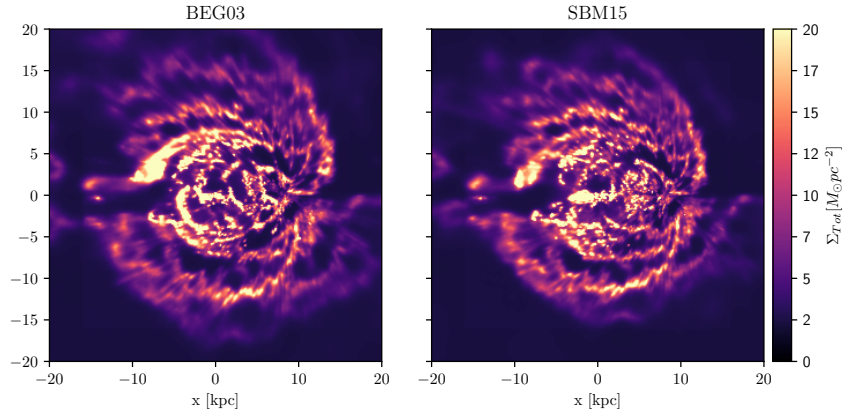


**Figure 1:** Total proton surface density used in our simulations for the introduced models.

CR distributions are obtained from solving the transport equations for energies ranging from 10 MeV to 1000 TeV on a logarithmic scale. Simulations are performed in a spatially advectionless setup with a constant diffusion coefficient. Transport is simulated with a global isotropic diffusion coefficient and an Alfvén velocity of  $D_{xx} = 5.52 \times 10^{28} \text{ m}^2 \text{ s}^{-1}$ ,  $v_A = 34.67 \text{ km s}^{-1}$  and  $D_{xx} = 5.33 \times 10^{28} \text{ m}^2 \text{ s}^{-1}$ ,  $v_A = 34.07 \text{ km s}^{-1}$  for BEG03 and SBM15, respectively.

From the simulated distributions, CR spectra for chosen primaries and secondaries ( Here: Carbon, Boron and electrons) are extracted for their analysis at Earth’s location. For the exact

location of Earth, the assumed position in the corresponding reconstruction is used (8.0 kpc for BEG03 and 8.15 kpc for SBM15).

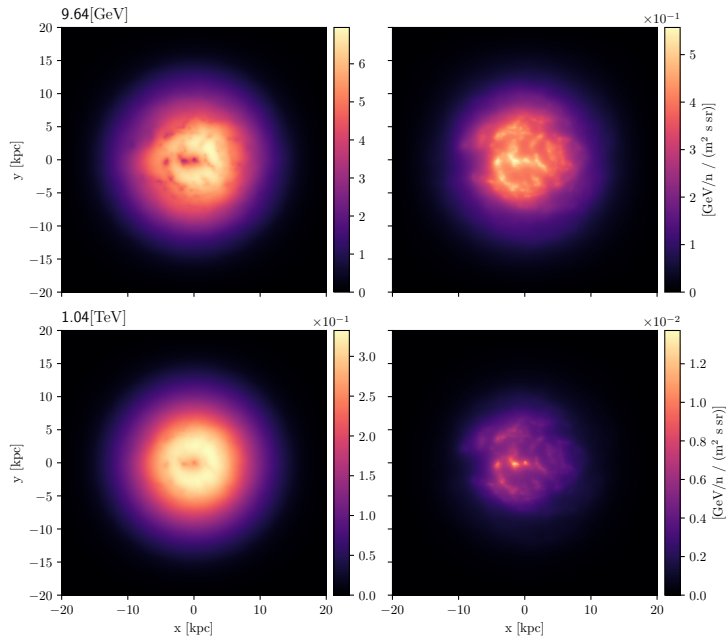
$\pi_0$ -decay, Bremsstrahlung and isotropic inverse compton (IC) emission are simulated as a second step in the analysis. As part of the computation for the  $\pi_0$  and Bremsstrahlung channels, emissivities per gas are produced and interpolated onto the gas reconstruction grid, where multiplication between the interpolated emissivities and the total gas distribution is performed. This way, the total gamma emission is generated by adding up the contribution for the different channels. Finally, a line of sight integral is performed to observe the specific structures introduced by the gas.

### 3. Results and Discussion

For this analysis, results are presented for the reconstructions from the BEG03 model only. First observing the variation on 3D spatial distributions of CRs, and then on the  $\gamma$ -emissivities

#### 3.1 Cosmic-Ray Distributions and Spectra

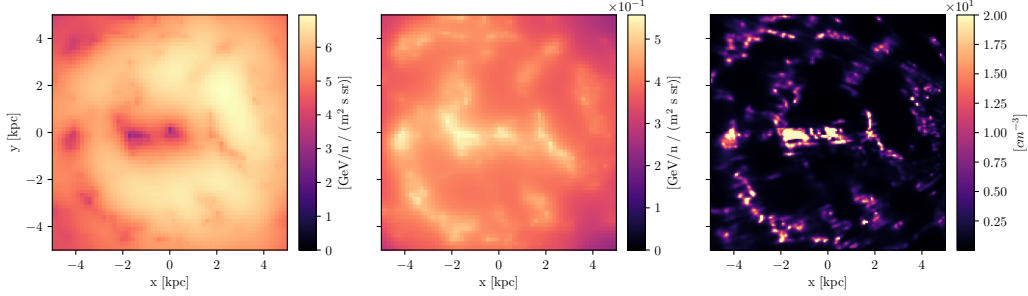
The introduced gas reconstructions imprint their structure in the distribution of CRs, as sources of secondaries due to spallation of primaries occurring in dense gas regions. By the same mechanism, structure is also introduced onto primaries of lower energy levels, where dense gas regions act as sinks. Here, the axisymmetric nature of the source model allows for these effects to be seen.



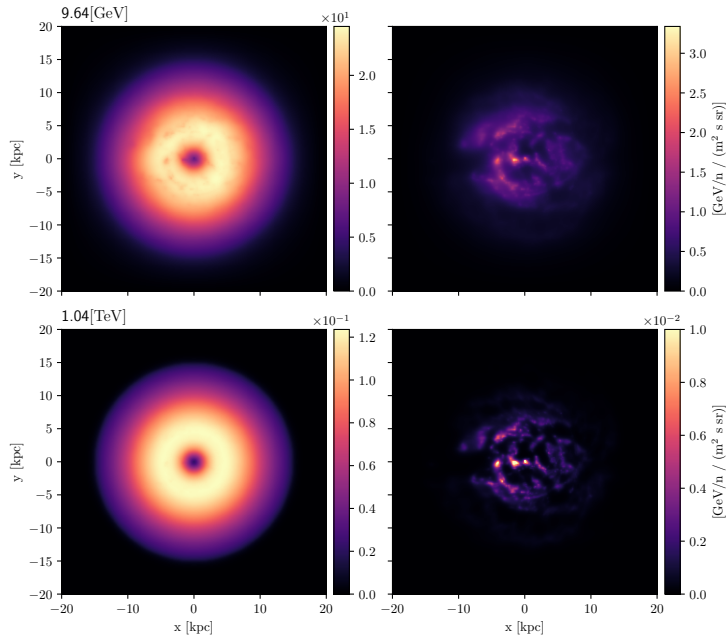
**Figure 2:** Galactic midplane  $x - y$  slice for Carbon 12 (left) and Boron 10 (right) distributions at 9.64 GeV and 1.04 TeV energy levels

Figure 2 shows the impact of the gas reconstructions on Carbon 12 and Boron 10, used as probes of effects on primary and secondary CRs respectively. For Carbon 12, the presence of under populated regions is directly correlated to over dense gas regions. Such an effect is notable at the

Galactic center, as shown in Figure 3 where such structures become more apparent. Boron 10 exhibits structure introduced by the gas model throughout all energies and features from the total gas distribution are retained. Its over populated regions are directly correlated to over dense regions in the total gas due to spallation of primaries.



**Figure 3:** Close up of Galactic midplane slices for Carbon 12 (left) and Boron 10 (center) distributions at 10 GeV compared to the same close up for the total gas distribution (right). Results are shown for a  $10 \text{ kpc}^2$  region around the Galactic center.



**Figure 4:** Galactic midplane  $x - y$  slice for primary (left) and secondary (right) electron distributions at 9.64 GeV and 1.04 TeV energy levels.

The regions of greatest density in the total gas distribution remain present on Carbon 12 across a wide energy band, with structures observable up to 1 TeV. In such dense regions, primary particles are subject to fragmentation loss processes by scattering with gas, where secondaries are produced as a result. This is further supported by the overlap between over-populated secondary regions with under-populated primary regions. As energy increases, spatial diffusion effects start to dominate and under-populated primary regions cease to depend on the presence of gas.

Primary and secondary electrons are shown in Figure 4. The impact of the new gas distribution is again present, yet structures do not persist up to 1 TeV for primary electrons. The 10 GeV energy bin for electrons exhibits less structure than in the Boron 10 case. The same is also true for primary electrons in comparison to Carbon 12. Secondary electrons over-populate the region at the galactic center, where they remain directly correlated to over-dense gas regions, as free electrons are produced from nuclei scattering in the gas region. In contrast, the under populated regions at 10 GeV account for electron energy loss processes, which are greater in dense gas locations.

We also observe that electron distributions do not diffuse over large distances like Boron and Carbon do. Hence, the axisymmetric ring shape for primary sources is strongly preserved, as well as the sharp features of the gas distribution for secondaries.

In Figure 5, we show the B/C ratio along with individual spectra measured at Earth. Here, we show local interstellar spectra without heliospheric modulation. In comparison to a simulation where our axisymmetric gas models are used instead and transport parameters remain equal, we observe an overall shift upward for the B/C ratio.

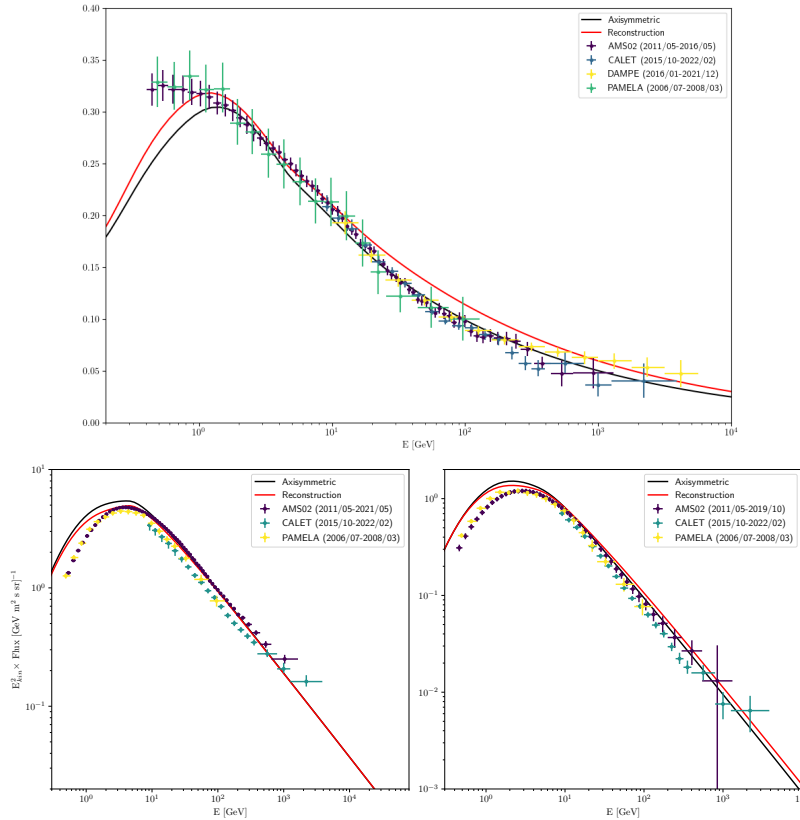


**Figure 5:** Top: B/C ratio at Earth. Bottom: Total Boron (left) and Carbon (right) spectra at Earth. Datasets: AMS 02 (2011/05-2021/05) [3] CALET (2015/10-2022/02) [2], PAMELA (2006/07-2008/03) [1]

The nature of the upward shift in the B/C ratio can be studied from the individual Boron and Carbon spectra. In comparison to the axisymmetric setup, a softening of the spectra for the reconstruction case is observed at the lower energies up to  $\approx 20$  GeV, where a higher deviation for the primaries is observed. For higher energies, primaries from the reconstruction and axisymmetric

setups remain in close agreement, whereas secondaries from the reconstruction setup show a hardening that persists as energy increases. As a result of this, there is an overall higher population of secondaries introduced through spallation, which leads to a lower population of secondaries via the same mechanism. This effect can be addressed by further tuning of the transport parameters, as well as the injection spectra for particles.

### 3.2 Gamma Emission

With the simulated distributions of CRs, gamma emissivities are computed. Figure 6 shows all sky maps for  $\pi_0$ -decay and Bremsstrahlung emission, along with total gamma emission. The total emission additionally includes contributions from IC emission. The effect on local emissivities for IC is shown in figure 7.

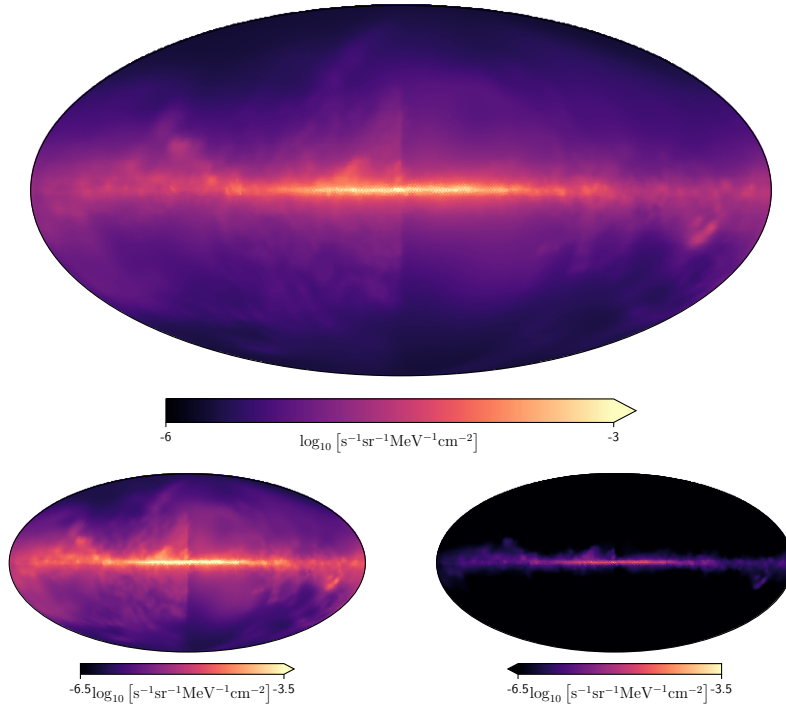


**Figure 6:** All sky gamma-ray emission at 1 TeV for an observer on Earth in the BEG03 model. Top: Total simulated emission. Bottom left:  $\pi_0$ -decay channel. Bottom right: Bremsstrahlung channel.

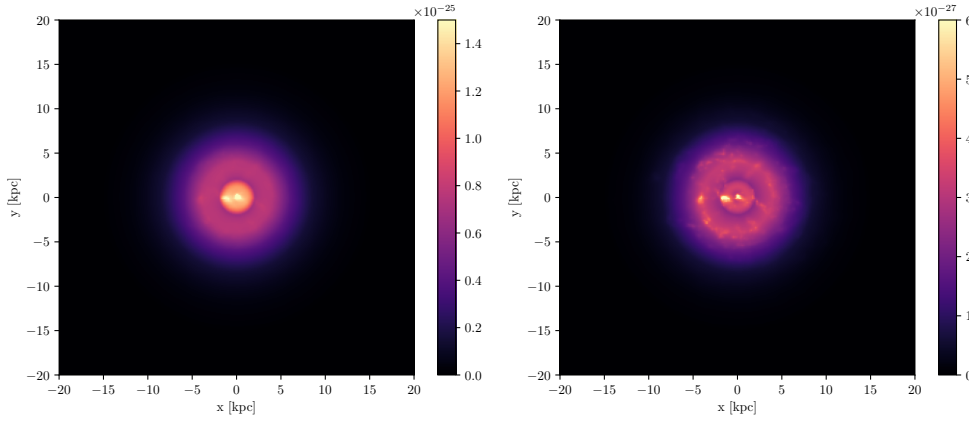


**Figure 7:** Galactic midplane  $x - y$  slices for IC emission. Left: Emission at 10 GeV. Right: Emission at 1 TeV.

$\pi_0$ -decay dominates over Bremsstrahlung and IC emission, it approximately follows the gas structure, as it results from a two-fold gas effect: through transport and through multiplication with the gas itself. Structures on the sky are entirely dominated by the gas reconstruction. Bremsstrahlung emission contributes mainly at the galactic plane, making this region brighter for the total  $\gamma$ -ray emission map, than in the  $\pi_0$ -decay channel.

Since no ring model is introduced, all sky maps result from a direct line of sight integration in the spherical domain. In contrast to ring models, features do not possess a high angular resolution, as they are constrained by the 3D grid resolution on which the gas is defined. Furthermore, as emissivities from transport are fully structure, there is no near-far ambiguity with respect to the gas model, and any galactic location can be analysed.

Local structures for IC emission retain phenomena visible in the CR distributions, as can be observed from the Galactic center region at 1 TeV, and the surrounding ring-like region around it where anisotropies arise. Features are present at the Galactic center as well for emission at 10 GeV. In contrast to CR distributions, gas structures are displayed sharply at higher energies instead of lower energies. This results from leptons being unable to diffuse for longer lengths at higher energies, producing high energy photons in a more compact region, which is defined by dense gas locations.

#### 4. Summary and Conclusions

The new 3D gas distributions introduce their structures on both primary and secondary species. For primary species, where over-dense regions produce an under population of primaries. The denser the gas is in a region, the more these features persist to higher energies. This effect comes as a result of spallation (nuclei) and energy losses (electrons) taking place where more gas is present. Such losses result in the production of secondaries as fragmentation and ionisation take place, making regions where gas is present effective secondary particle sources.

The comparison between axisymmetric and reconstructed spectra further reflect the primary-secondary anti correlation as secondary spectra hardens. Since overall a higher population of secondaries than primaries is observed in the B/C ratio, this shift can be addressed through further

tuning of transport parameters and injection spectra. Although results are not presented with a force field modulation, lower energy ranges for data are fitted by its introduction.

Local and line-of-sight integrated gamma-ray emission are affected by the gas. The all sky maps reflect the inherent gas structures and highlight features that result from emission in dense gas regions. Structures are directly imprinted by the gas through transport and multiplication with the gas. In particular, local emissivities for IC emission exhibit gas structures at higher energies, in contrast to CR distributions, due to energy losses correlating IC emission to the gas.

## References

- [1] O. Adriani et al. Measurement of Boron and Carbon Fluxes in Cosmic Rays with the PAMELA Experiment. *ApJ*, 791(2):93, August 2014.
- [2] O. Adriani et al. Cosmic-Ray Boron Flux Measured from 8.4 GeV/n to 3.8 TeV/n with the Calorimetric Electron Telescope on the International Space Station. *prl*, 129(25):251103, December 2022.
- [3] M. Aguilar et al. Properties of Cosmic-Ray Sulfur and Determination of the Composition of Primary Cosmic-Ray Carbon, Neon, Magnesium, and Sulfur: Ten-Year Results from the Alpha Magnetic Spectrometer. , 130(21):211002, May 2023.
- [4] Carmelo Evoli, Daniele Gaggero, Andrea Vittino, Giuseppe Di Bernardo, Mattia Di Mauro, Arianna Ligorini, Piero Ullio, and Dario Grasso. Cosmic-ray propagation with dragon2: I. numerical solver and astrophysical ingredients. *Journal of Cosmology and Astroparticle Physics*, 2017(02):015, feb 2017.
- [5] Guðlaugur Jóhannesson, Troy A. Porter, and Igor V. Moskalenko. *ApJ*, 856(1):45, mar 2018.
- [6] R. Kissmann. Picard: A novel code for the galactic cosmic ray propagation problem. *Astroparticle Physics*, 55:37–50, 2014.
- [7] David Maurin. usine: Semi-analytical models for galactic cosmic-ray propagation. *Computer Physics Communications*, 247:106942, 2020.
- [8] Mertsch, P. and Phan, V. H. M. Bayesian inference of three-dimensional gas maps - ii. galactic hi. *A&A*, 671:A54, 2023.
- [9] Mertsch, P. and Vittino, A. Bayesian inference of three-dimensional gas maps - i. galactic co. *A&A*, 655:A64, 2021.
- [10] T. A. Porter, G. Jóhannesson, and I. V. Moskalenko. The galprop cosmic-ray propagation and nonthermal emissions framework: Release v57. *The Astrophysical Journal Supplement Series*, 262(1):30, sep 2022.